Proceedings of the ASME 2019 38th International Conference on Ocean, Offshore and Arctic Engineering
OMAE2019
June 9-14, 2019, Glasgow, Scotland, UK

Draft - OMAE2019-96753

EXPERIMENTAL AND NUMERICAL STUDY ON THE HYDRODYNAMIC PROPERTIES OF A SIMPLIFIED FLOATING HYDROCARBON STORAGE FACILITY

Chi Zhang
Department of Civil and Environmental Engineering, Faculty of Engineering, National University of Singapore

Nuno Fonseca
SINTEF Ocean
Trondheim, Norway

Allan R. Magee
Department of Civil and Environmental Engineering, Faculty of Engineering, National University of Singapore

Nianxin Ren
Department of Civil and Environmental Engineering, Faculty of Engineering, National University of Singapore

ABSTRACT

A compliant modular floating hydrocarbon storage facility (FHSF) has been proposed for ocean space utilization. The FHSF consists of many floating hydrocarbon storage tanks (FHST) and several surrounding barges. These modules are connected in proximity through soft mooring system which reduces the environmental loads significantly. However, there are concerns on the potential resonance in the narrow gaps and the strong hydrodynamic interactions. This paper focuses on the hydrodynamic properties of a simplified subsystem which qualitatively represents part of the behavior of the entire FHSF but with reduced complexity. This subsystem consists of two FHSTs and a barge frame and is suitable for evaluating numerical analysis tools. Experimental studies on the subsystem and the complete system were performed in the ocean basin in SINTEF Ocean. A series of random, wide-band and realistic random wave tests were carried out to generate benchmark data to verify numerical analysis tools. Empty, partially loaded and fully loaded conditions were tested. The free surface elevations in the narrow gap and in the internal tank were obtained. A frequency domain numerical model of the subsystem was established in WAMIT based on linear potential theory. Higher order boundary element method (HOBEM) has been utilized to improve the accuracy and convergence. The influence of internal liquid (sloshing) inside the tanks is also considered in the linear range. The mooring system is simplified as linear springs. Linearized damping is introduced. The response amplitude operators (RAOs) of 6 degrees of freedom (D.O.F) and free surface elevations from numerical and experimental studies under the head sea conditions are compared. Good agreement on the motion RAOs are found, but significant differences are found on the RAOs of the elevation of the free surface. Finally, the influence of significant gap resonances is used to generate insight into how these problems might be mitigated.

KEYWORDS

Floating structure, Ocean space utilization, Hydrodynamic interactions, Gap resonances, Hydrocarbon storage.

NOMENCLATURE

COG	Center of gravity
R_{xx}, R_{yy}, R_{zz}	The radius of gyration in x, y, and z
T_p	Peak period
H_s	Significant wave height
RAO	Response amplitude operator
∅	Velocity potential
ω	Wave frequency
M	The inertia matrix of the floating body
A	Added mass matrix
B	Potential damping matrix
C	Restoring matrix
C_{ext}	External stiffness matrix
F	Wave excitation force vector

INTRODUCTION

Ocean space utilization is an important topic in offshore industry. After long-term land reclamation in the coastal area, the environmental impact is a concern. Constructing floating structures can be one solution to the issue. Floating structure can be constructed in both near-shore and offshore area with a properly designed mooring system. To reduce the construction cost, it can be designed and constructed in modules. There have been many concepts and applications of modular floating structure for ocean space utilization. For example, the floating performance platform has been constructed in Marina Bay in Singapore [1]; the floating oil storage base in Japan [2] has served for more than 10 years, and the recent research work was done on the floating bridges in Norway [3]. The recent applications of VLFS were reviewed in [4]. These new concepts always contain innovations in their design.

The hydrodynamic responses are critical to justify the feasibility and reliability of the VLFS concepts. For continuous large floating structure, hydroelastic analysis has been adopted to solve the fluid-structure-interaction problem [5-7]. This method can also be applied to the modular floating structures, but the narrow gaps between modules are always omitted. A more general and straightforward method is based on rigid body flexible connector assumption (RMFC) [8-10]. The single module is considered as a rigid body, and the modules are interconnected through different types of flexible connectors. The hydrodynamic problem can be solved with conventional numerical tools if the body number is limited. When there is a large number of bodies, the solving procedure can be very slow due to a large number of degrees of freedom. Advanced methods such as higher order boundary element method can be more robust than the conventional method [11]. A more recent method proposed by Zhang et al. is based on nonlinear network theory [12]. The dynamic responses of the multimodule VLFS can be solved, and the method has been verified by model test.

The floating hydrocarbon storage facility is one of the innovative modular designed floating structure as shown in Fig. 1. It has a design life of 60 years and a storage capacity of 30,000 m^3. The hydrocarbon products will be stored in the modular designed floating hydrocarbon storage tanks. The FHSTs will be moored to the surrounding floating barges through special designed soft mooring system [13]. The entire system is designed to be compliant to reduce environmental loads. A detailed description of the conceptual design of the FHSF system can also be found in [13]. The concept of FHST has been proven as a success in the design sea states around Singapore. Both hydrostatic and hydrodynamic performances of the single FHST are satisfactory [14]. However, it is still challenging to evaluate the performance of the complete system. The FHSF has several features which are different from the concepts reviewed above. Firstly, it consists of more than 30 bodies, and each body has complex shapes. This increases the difficulties on the hydrodynamic analysis. In addition, there exist narrow gaps between those bodies. These complicated features are rarely discussed or considered in the previous studies. To reasonably evaluate this innovative concept, both experimental and numerical simulations are critical.

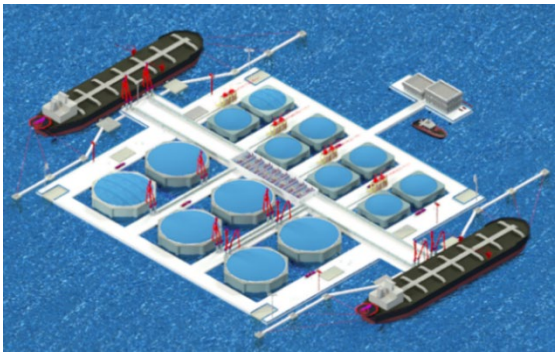

Figure 1: Conceptual design of the FHSF.

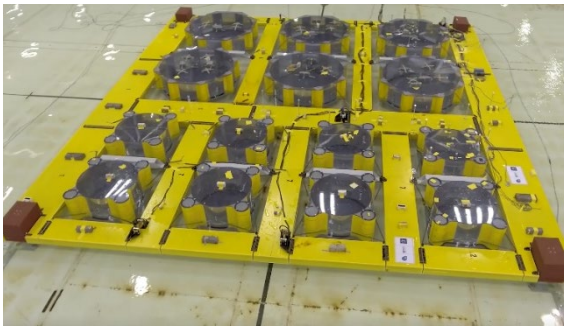

Figure 2: Physical model of the FHSF in the ocean basin.

To reduce the uncertainty in the analysis, a simplified system consisting of two FHST and floating barge frame is used. It represents the main features of the complete system. The simplified system will be investigated first to understand the behavior of the system. The model test and numerical analysis are accordingly divided into two phases. In Phase-1, the simplified system was simulated for both conceptual and numerical validation. In Phase-2, the complete system is tested [15]. Figure 2 shows the physical model in Phase-2. The numerical simulation of the entire system will be extended from the simplified system in the future.

In this paper, the simplified system will be introduced first. The model test configuration and the numerical model of this system are presented. The model test configuration in Phase-2 will be introduced separately in another paper. The comparison between numerical and experimental results will be discussed. The main conclusions and future work will be summarized in the final part. The focus of this paper is to validate the numerical model in various loading conditions. The second order responses are not covered in this paper. The environmental condition in the nearshore is very mild, thus the second order. Due to the page limitation, only selected cases will be discussed.

DESCRIPTION ON THE SIMPLIFIED FHSF SYSTEM

The simplified system contains two FHSTs of smaller size and a rigid barge frame. The storage capacity of the FHST is 12500m^3.

The two FHSTs are connected to the surrounding barge frame through 8 flexible ropes. The position of the fairlead points and the anchor points are shown in Fig. 3. In the entire system, the barges are interconnected through flexible connectors. In the present study, the barge frame is considered as one rigid body. The interconnection loads between barges are measured in model test Phase-2. The prototype dimensions of the FHST and the barge frame can be found in Table 1 and 2. Their mass properties can be found in Table 3 and 4 respectively. In Table 3 and Table 4, the vertical center of gravity (COG) is measured from the lower surface of the bottom slab. The moment of inertia is determined with reference to a coordinate system with the same axis definition as explained in the model test setup but with the origin at the COG. The barge frame is assumed to be free floating vertically. No motion is allowed in the surge, sway, and yaw in both numerical and experimental study. The horizontal motion of the barge frame is restrained by mooring dolphins as in the entire system. In the prototype, an articulated bridge is located in the barge center to protect the FHSTs. In the simplified system, this bridge has been moved to above of the free surface.

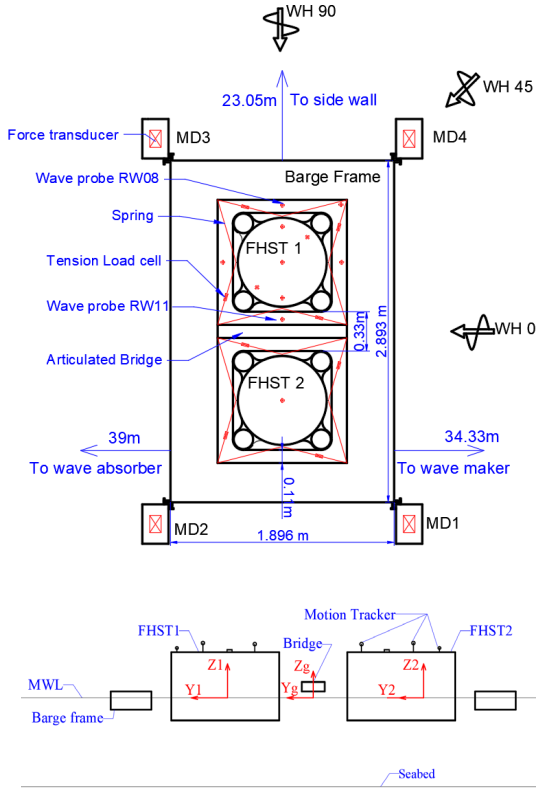

Figure 3: Configuration of the simplified FHSF system.

The simplified system has reduced the complexity significantly. It keeps the critical features of the FHSF such as the narrow gaps, the mooring system, and the hydrodynamic interactions. Here, one may be confused about moonpool and narrow gaps. Molin pointed out the differences between these two [16]. According to his definition, the narrow gaps in the FHSF should be a moonpool of irregular shape, but no strict differentiation will be made in this paper. Both experimental and numerical model were built with a similar setup. It reduces complexity for the experiment and simulation significantly. Also, it makes the interpretation of the results easier for the entire system.

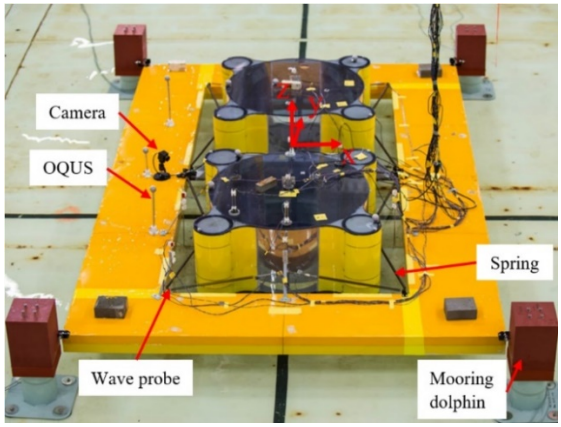

Figure 4: Model test setup in the ocean basin.

MODEL TEST SETUP

The model tests are designed under a Froude scaling factor of 1:45. The dimensions and mass properties of the FSHT and barge frame in model scale are listed in Table 1-4 respectively. The mooring ropes are modeled by linear springs but with a similar configuration as in the prototype. The load cells are embedded into the mooring dolphins so that the global horizontal loads on them can be obtained. The model can be rotated so that different incident wave headings can be tested. In this model test, waves from 0 deg, 45 deg, and 90 deg are considered. The definition of these wave heading is shown in Fig. 3. They are denoted as the head sea, oblique sea, and the beam sea conditions respectively. In this paper, only the head sea condition will be discussed. The loading conditions are defined as the filling ratio of the designed storage capacity. Empty, 20% filling ratio and 100% filling ratio of the designed storage capacity were tested. The latter two are also denoted as partially loaded and fully loaded cases. The internal liquid is simulated by fresh water. The mass of the hydrocarbon products is scaled down to the model scale.

The model tests were performed in the ocean basin at SINTEF Ocean. The basin has a length and width of 80m and 50m respectively. The depth of the basin is 10m, but the water depth can be adjusted by moving the adjustable floor. The water depth can vary from 0m to 8.7m. During the model test, the water depth was adjusted to 0.45m corresponding to a design water depth of 18m. The double-hinged wave paddles and the passive wave absorbers are installed on the two ends of the basin. The current can be generated in line with the incident waves. The model is placed in the middle of the basin 35.28m from the wave maker. The 6 D.O.F motions of the two tanks and the barge frame are monitored by the motion tracking system OQUS. The connection forces and the forces on the mooring dolphins were measured through load cells. 11 wave probes are installed to monitor the free surface elevation in the basin, in the narrow gaps and inside

the inner tanks of the FHSTs. The positions of those wave probes can be found in Fig. 3. The Figure identifies only relative wave 8 (RW8) and RW11, since the paper discusses results from these two sensors only. In the model test, the origin of the body-fixed coordinates locates at the center of each body's water plane. The x-axis points towards the wave maker, the z-axis points upwards and the y-axis can be determined by right-hand rule. The global coordinate aligns with the body-fixed coordinate system. The detailed definition can be found in Fig.3. In the numerical model, the same coordinate system is defined. There are three cameras mounted in the front, on the side and under water of the model. One more camera was mounted on the barge frame to record the elevation of the free surface. All the systems are synchronized with a sampling frequency at 20 Hz.

Table 1: Geometrical dimensions of the FHST in the prototype and model scale (Unit: m)

Dimension	Prototype	Model
Total height	22.60	0.4144
Length/width (edge to edge)	37.63	0.8362
Overall diameter	33.90	0.7533
Internal clear diameter	33.00	0.7333
Diameter of the floater	7.980	-
Bottom slab thickness	0.75	0.0150
Draft (empty)	6.22	0.1382
Draft (20% filling)	8.08	0.1795
Draft (100% filling)	15.50	0.3444

Table 2: Geometrical dimensions of the barge frame in the prototype and model scale (Unit: m)

Parameter	Prototype	Model
Length (exterior)	130.20	2.8933
Length (interior)	100.20	2.2267
Width (exterior)	85.30	1.8956
Width (interior)	49.30	1.0956
Depth	6.00	0.1333
Draft	4.00	0.0890

Table 3: Mass properties of the FHST in the prototype and model scale

Parameter	Prototype	Model	Unit
Mass (empty)	7,494,737	79.0-79.5	kg
R_{xx}/R_{yy} (empty)	15.06	0.318	m
R_{zz}(empty)	16.33	0.406	m
Vertical COG	8.17	0.168	m
Mass (20%)	9,669,737	-	kg
Mass (100%)	18,119,737	-	kg

Table 4: Mass properties of the barge frame in the prototype and model scale

Parameter	Parameter	Prototype	Unit
Total mass	24,938,634	267	kg
Vertical COG	3.42	0.076	m
R_{xx}	44.35	0.986	m
R_{yy}	30.85	0.686	m
R_{zz}	42.47	0.944s	m

The environmental conditions include regular waves, random wave tests to simulate the design 1-year and 100-year storm and white noise tests. The environmental conditions and corresponding parameters are summarized in Table 5. The 1-year storm is quite mild, so it will not be discussed in this paper. Combined 100-year wave and 100-year current test was also performed to validate the concept. It will not be included in this paper as our numerical method can only consider wave effects at this stage. JONSWAP spectrum is assumed for the 100-year waves. The white noise tests are performed to obtain the RAOs of the system for numerical validation. The H_s of the white noise is 2m, and the wave period varies from 4s to 20s which is sufficient to cover the wave frequency range around Singapore.

Table 5: 1-year and 100-year sea states at a specific position around Singapore and the white noise parameters

Return periods	H_s (m)	T_p (s)
1 year	1.0	5.0
100 year	1.8	7.0
White noise	2.0	4 to 20

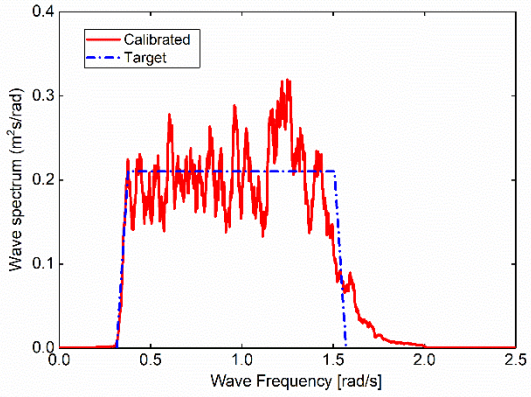

Figure 5: Model test setup in the ocean basin.

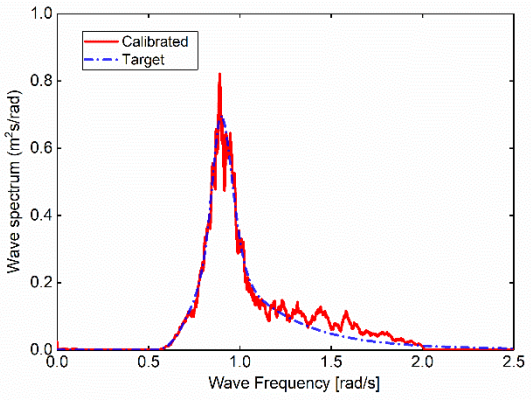

Figure 6: Model test setup in the ocean basin.

In the model test, both white noise and random wave tests last for 3 hours in the prototype. The theoretical and calibrated incident wave spectrum of white noise and 100-year waves are plotted in Fig. 5 and Fig. 6 respectively. Good agreement can be found from the comparison. The model tests results are selected after the motion reach the steady state to calculate the RAOs. The RAOs are calculated based on the equation below.

$$\boldsymbol{RAO} = \sqrt{\boldsymbol{S_r/S_I}} \qquad \text{Eq. 1}$$

in which is the S_r is response spectrum and S_I is the incident wave spectrum. Both spectra are derived from the recorded time history. Threshold has been set for the incident wave spectrum, when the wave energy is below the threshold, the RAOs are not used to control the quality of the results. Both RAOs and the statistical results are transferred back to full scale to compare with the numerical results. That is to say, the results in this paper are all in full scale unless otherwise specified.

NUMERICAL MODEL

Numerical model on the simplified system was built based on linear potential theory. The velocity potential $\emptyset$ governed by Laplace's equation in the fluid domain can be solved with proper defined boundary conditions. The detailed definition of the boundary value problem (BVP) for a floating body can be found in [17]. The velocity potential $\emptyset$ is normally decomposed into incident wave potential $\emptyset_I$, scattered potential $\emptyset_s$, radiation potential in N D.O.Fs. $\sum_{i=1}^{N} \emptyset_i$ as shown in Eq. 2. The incident wave potential and scattered potential are usually combined as diffraction potential $\emptyset_D$.

$$\emptyset = \emptyset_I + \emptyset_s + \sum_{i=1}^{N} \emptyset_i \qquad \text{Eq. 2}$$

For a single body, N equals 6 in the above equation. For the multibody system, it is straightforward to solve the radiation problem by extending N from 6 to $\mathbf{6 \times N}$ [8]. To solve the boundary value problems, Green's theorem is applied to derive integral equations. By using HOBEM, B-splines are utilized to describe each patch of the body. This is also in an equivalent manner to the representation of the velocity potential. As commented in [17], the higher-order method is more efficient and accurate in most cases. Another advance function applied in this numerical model is the thin submerged elements. The bottom skirt which a thin plate on the bottom as shown in Fig. 7 in light blue color, and it has been proven to improve the hydrodynamic responses. The bottom skirts are modeled by thin submerged elements with 'dipole' method. At this stage, the effects of fluid in the internal tanks are also considered, but the sloshing can only be considered in linear range. The details on these advanced functions can be found in [18]. Once radiation and diffraction potentials are solved, the added mass and potential damping coefficient and the first-order wave excitation forces can be expressed as Eq.3 to Eq.4.

$$\boldsymbol{A_{ij} - \frac{i}{\omega} B_{ij} = \rho \iint_{S_b} n_i \emptyset_j dS} \qquad \text{Eq. 3}$$

$$\boldsymbol{F_i = -i\omega\rho \iint_{S_b} n_i \emptyset_D dS} \qquad \text{Eq. 4}$$

where $\boldsymbol{F_i}$ is the wave excitation force in the i[th] mode of motion, $\boldsymbol{A_{ij}}$ and $\boldsymbol{B_{ij}}$ are the added mass and radiation damping in i[th] mode induced by the motion in j[th] mode. S is the wet surface of the floating body, $\boldsymbol{n_i}$ is the normal vector of the wetted surface, $\boldsymbol{\rho}$ and ω are the water density and wave frequency.

For a rigid floating system with zero forward speed in waves moving in the steady state, the equation of motion [17] due to first-order wave excitations can be described in the frequency domain in Eq. 5,

$$\boldsymbol{-\omega^2 \left(M + A(\omega)\right)X(\omega) + i\omega(B(\omega) + B_{ext})X(\omega) + (C + C_{ext})X(\omega) = F(\omega)} \qquad \text{Eq. 5}$$

where ω is the wave frequency; M is the structural mass matrix; **A**(ω) and **B**(ω) are the frequency dependent added mass and damping matrix respectively; $\boldsymbol{C}$ is the restoring matrix; $\boldsymbol{B_{ext}}$ and $\boldsymbol{C_{ext}}$ are the additional damping matrix and external restoring matrix; **X**(ω) is the motion vector; **F**(ω) is the external force vector. All the vectors and matrices are expressed in the frequency domain. So, the motion RAOs in linear range can be solved efficiently.

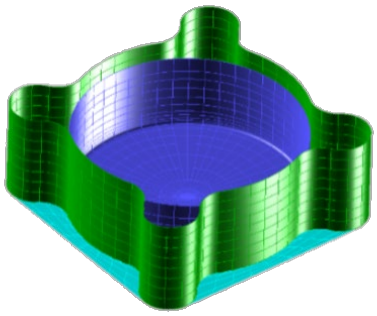

Figure 7: Numerical model of the FHST.

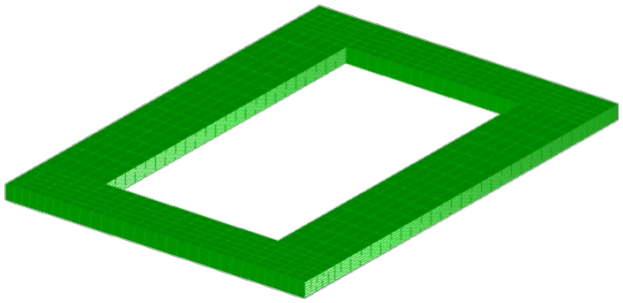

Figure 8: Numerical model of the barge frame (the scale has been adjusted for ease of viewing).

The numerical model was built in WAMIT v7.2 [18] with the same setup as in the model test. The meshes of the FHST and the barge frame is shown in Fig. 7 and Fig. 8 respectively. The side wall and bottom slab of the FHST are represented by 16 patches and the bottom skirts are represented by 8 dipole patches. internal tank is represented by 8 patches. For each patch, there are 36 sub-panels. All the patches are described by 3rd order B-splines. Convergence tests have been performed before moving forward. In the simplified system, the soft mooring system provides additional restoring forces. The mooring system provides additional stiffness in surge and sway. It was simplified as equivalent linear spring in the numerical model. The equivalent stiffness is 1200 kN/m in the prototype. To damp the unrealistic motions in near resonance frequencies, linear damping ratio of 10% is introduced on pitch and roll. 10% of heave critical damping is also introduced to include the damping effect induced by the bottom skirts. Both damping ratios are estimated and linearized based on the decay test performed on a single FHST. As there exists narrow gaps and sloshing, the frequency interval is set to be 0.01 rad/s between 0.2 rad/s to 2 rad/s to capture the resonant phenomenon precisely. At this stage, no free surface damping has been introduced either inside the tank or in the narrow gaps. The effects of this will be discussed later.

RESULTS AND DISCUSSIONS

Comparison of RAOs of the barge frame in the head sea

Figure 9 and 10 show the RAOs of the barge frame in heave and pitch under different loading conditions of the FHST. In these figures, FL00 stands for the empty loaded case, FL20 stands for 20% filling ratio case, FL100 represents the fully loaded case. Similar definitions are adopted in all the remaining figures in this paper. The RAOs are plotted from 2s to 16s which covers the wave frequency range. Very good agreement can be found between numerical and experimental results especially in pitch. The heave RAOs tend to be overestimated at around 6s to 6.5s. The overestimation might be related to the gap resonances in the narrow gaps. It is expected to be improved once the free surface damping is introduced.

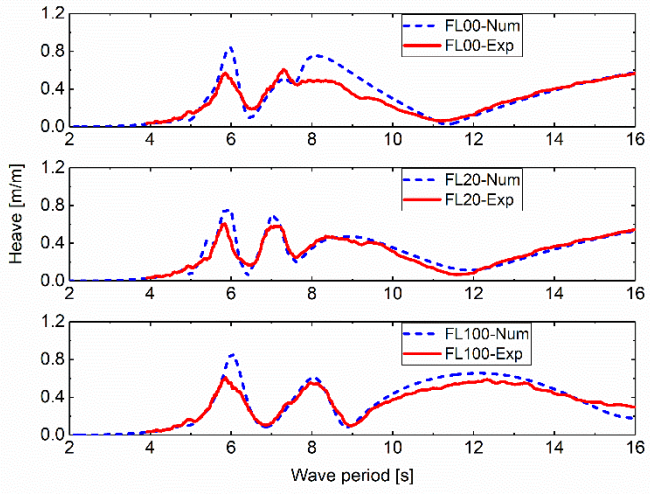

Figure 9: RAOs of the barge frame in heave

The canceling period can be found on the RAOs in both pitch and heave at around 6.5s to 7s. The wave length of the incident wave with a period at around 6.5s to 7s is close to the length of the barge frame. The force on the two transverse parts of the barge frame can cancel with each other. The knockout is also sensitive to the draft of the FHST. Comparing the RAOs in heave in the empty, partially and fully loaded cases, it is obvious to see the translation of the knockout point towards larger wave periods. A stronger hydrodynamic influence from the FHSTs on the barge frame is suspected to be the reason. The draft of the FHST under the fully loaded case is much larger than those in the empty and partially loaded case. The results also show that the motions of the barge frame are quite small in the wave frequency range. In all the 3 loading conditions, the maximum RAOs in heave and pitch are smaller than 0.8 m/m and 2.0 deg/m respectively. The amplitudes of the RAO are not sensitive to the loading condition of the FHST. The mild motions of the barge frame are important for the operation.

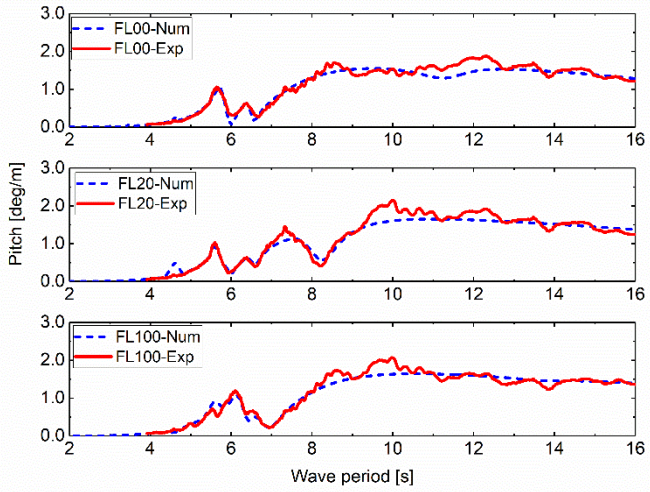

Figure 10: RAOs of the barge frame in pitch

Comparison of RAOs of FHST in the empty condition in the head sea

Figure 11 and 12 show the RAOs of two FHSTs in translational and rotational directions for the empty case. In these figures, TNK1 and TNK2 stand for FHST 1 and FHST 2 respectively. The positions of the two FHST are shown in Fig. 4. As the system is symmetrical, the motions of the two FHSTs are almost the same. Very good agreement was again found between the numerical and experimental results in surge, heave, and pitch. By introducing linear damping, the peak values in pitch and heave predicted by the numerical model are almost the same as those from the model test. This indicates the linear damping ratios have been properly selected.

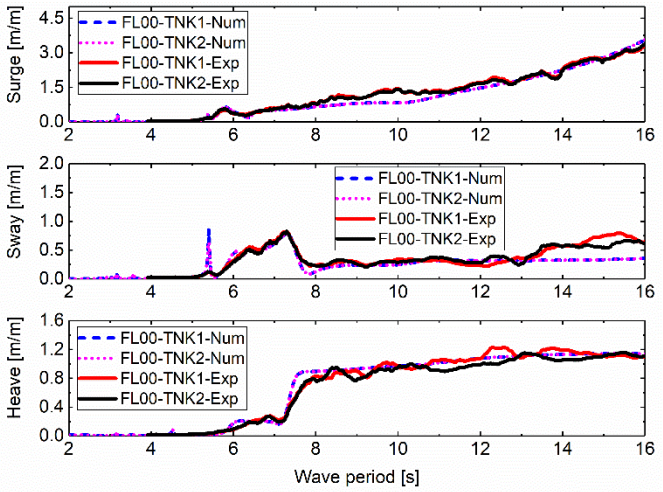

Figure 11: RAOs of the translational motions of the FHST in the empty case

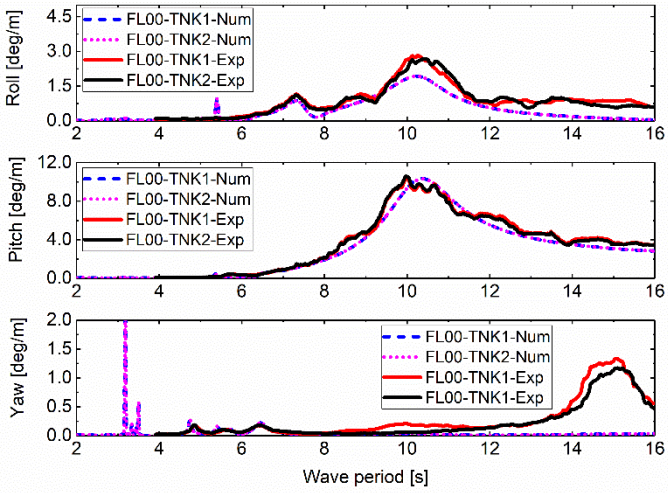

Figure 12: RAOs of the rotational motions of the FHST in the empty case

The numerical simulation also shows the accurate prediction of the transverse motions such as sway and roll. These transverse motions are mainly generated by hydrodynamic interactions and influenced by the gap resonances between the two FHSTs. A noticeable peak can be found on the numerical results in sway at around 5.5s. This peak is due to the overestimation on the free surface elevation in the gaps when the resonance occurs. Similarly, the RAOs in roll also show peaks at the same period. The RAOs in yaw show differences between numerical and experimental results in short waves and in long waves. In short waves, the yaw RAOs are influenced by the unrealistic gap resonances in the numerical model. In longer waves, the difference is possibly due to the difference of the inertia of the FHST. It will not cause problem as the yaw motion is quite small.

Table 6: Natural period of surge, pitch and heave of the FSHT in the empty case

Modes of motion	Decay	RAO (experimental)	RAO (numerical)
Surge	19.2	1.0	5.0
Pitch	9.9	10.1	10.4
Heave	8.3	N.A.	N.A.

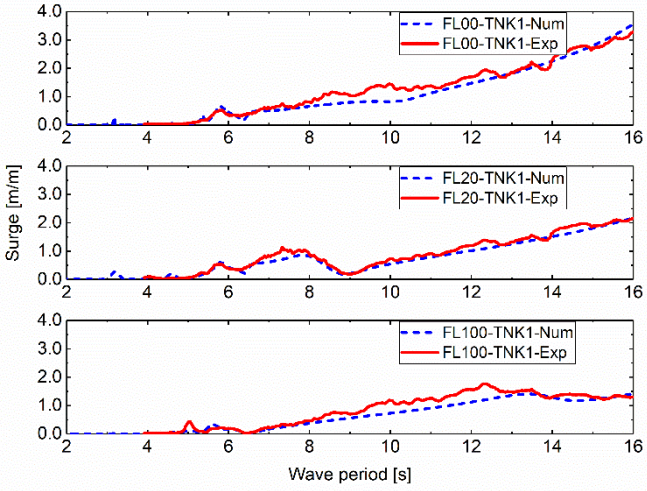

Figure 13: RAOs of the FHST in surge in the empty, partially loaded and fully loaded case

Table 6 shows the natural periods identified from the decay test in calm water and the peak period identified from both experimental and numerical RAOs. The decay test was done in calm water after the setup of the simplified system. The natural period of surge in the empty case is found to 19.2s which is not covered in the range of the RAO plot. It is far away from the peak period of the design sea states. The amplitude of the RAOs in surge is smaller than 1.0 m/m at around 7.0 s. It verifies the mooring system design is proper. The natural period of pitch identified from decay test is around 9.9s and the period of the peak in experimental and numerical RAOs is around 10.1s and 10.4s. The differences are less than 5%. The amplitude of pitch can be around 11 degree/m. As there still exist some wave energies around this wave period in the 100-year sea state as shown in Fig.3, results from the random wave test should be analyzed carefully. The RAOs in heave is smaller than 1.0 m/m

in the wave frequency range. Although there exist transverse motions, they are all in the acceptable range. In general, the results indicate the motions of the FHST in head sea is very mild in the empty case.

Comparison of RAOs of the FHST in partially and fully loaded conditions

The RAOs of the FHST in surge and pitch in the partially and fully loaded conditions are plotted in Fig.13 and Fig.14 respectively. The results in the empty case are also plotted for ease of comparison. The two FHSTs have similar RAOs, so only RAOs of one of the FHSTs are plotted. In general, the numerical simulation gives reasonable results in surge compared to the experimental results. In pitch, the numerical results are also comparable to the experimental results in the partially loaded case. The peak of the pitch has been shifted to 8s. It is closer to the peak period of the 100-year storm, so large pitch motion may be induced. So, for the extreme response analysis, this partially loaded case should be treated carefully. In the fully loaded case, the peak period of pitch has also been predicted accurately in the numerical simulation. However, the amplitude seems to be underestimated. In the fully loaded case, the bottom of the FHSTs is very close to the seabed. In such a case, vortex generated by the bottom skirts might be influenced by the seabed. More detailed analysis is necessary to explain the differences. It is not a concern as the peak period of pitch is around 14s the fully loaded condition which is even larger than the empty case.

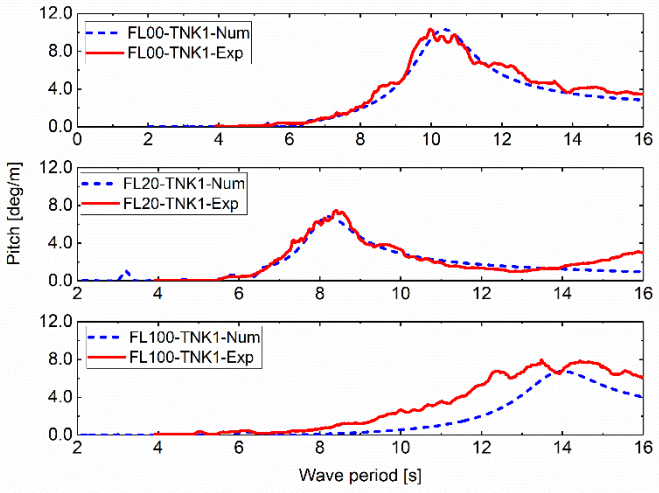

Figure 14: RAOs of the FHST in pitch in the empty, partially loaded and fully loaded case

Sloshing was a concern for the FHSF concept. Violent sloshing is not allowed for the hydrocarbon storage. No violent sloshing was found during the model test in both partially and fully loaded conditions. The linear sloshing model applied in the numerical model gives very promising results, although the results are not discussed in detail in the present paper. However, violent sloshing was observed during the previous model test for the single FHST with a storage capacity of 5000 m^3 [14]. The reduction on the sloshing severity may be caused by size increase of the FHST. The size of the internal tank of the FHST has been increased significantly from 25m to 33m. The volume of the stored liquid is also different although the percentage is kept the same at 20%. Both will change the natural frequency of the lowest sloshing mode that is well known related to the dimensions of the tank.

Comparison of the free surface elevation in the narrow gaps

The RAOs of the free surface elevations in the narrow gaps are obtained through the wave probes mounted on the barge frame. The results have been transferred to the global coordinate system. The RAOs of the free surface elevation in the central narrow gap at RW11 and the motion of the free surface in the side narrow gap at RW08 are plotted in Fig. 15 and 16. The positions of RW08 and RW11 can be found in Fig. 3. Strong fluctuations on the RAOs can be found in shorter waves. In both RW08 and RW11, there exist several peaks on the RAOs between 4s and 8s. These peaks correspond to the different modes of the free surface elevation in the narrow gaps. In the longer wave periods, the free surface elevation tends to be 1m/m because the incident waves can transmit the barge frame easily. From the model test results, it can be found that the maximum amplitude of the RAOs can reach 4m/m. The worst case is the fully loaded case. In the fully loaded case, the maximum peak value can be found at around 7s in RW08. Considering the 2 m freeboard of the barge frame, there will probably be green water on the deck for the design sea state. This problem should be improved in the future by increasing the free board of the barges.

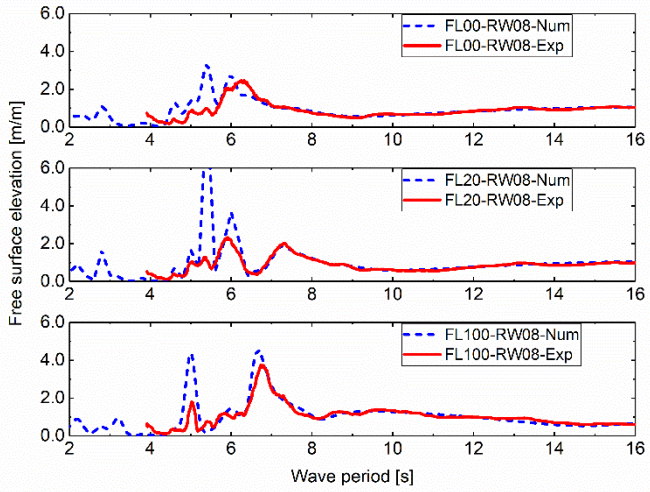

Figure 15: RAOs of the free surface elevation at position RW08 in the empty, partially loaded and fully loaded case

The numerical model tends to overestimate the RAOs of the free surface elevation. The overestimation of free surface elevation in the numerical simulation mainly occurs between 4s and 8s. This is as expected because no free surface damping was introduced. The overestimation in the numerical simulation can be 7 times that of the test results. However, not all the peak values have been overestimated. When the wave period is larger than 7s, the

numerical model gives quite consistent results. In addition, the numerical results show peaks at almost the same position as the experimental results. Based on this model, the free surface damping will be introduced in the future to give more accurate results on the free surface elevation.

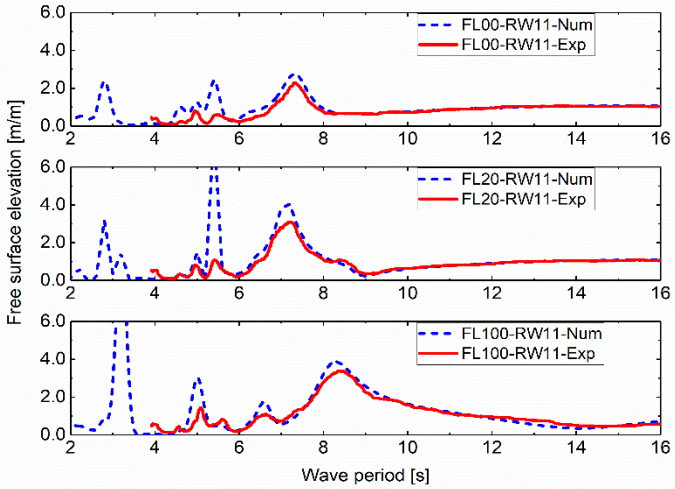

Figure 16: RAOs of the free surface elevation at position RW11 in the empty, partially loaded and fully loaded case

CONCLUSIONS

This paper introduced the floating hydrocarbon storage facility and its simplified system for numerical and experimental study. The simplified system contains the main feature of the entire system, while being much simpler to model and analyses. Modeling and validation for the simplified system is a step towards numerical modeling of the complete floating storage system. The model test setup and the numerical model have been introduced in detail. Comparison between numerical and experimental results are presented. The main findings are summarized as follow,

(1) Very good agreement was found between the RAOs of the motion of the barge frame and FHST obtained from the numerical and experimental study. One exception is the RAOs in pitch in the fully loaded condition when the FHST is very close to the seabed.

(2) The motion of the barge frame is mild. The RAOs of the FHST is also acceptable in the wave frequency range. The natural period of the surge of the FHST has been shifted outside wave frequency range. Design of the innovative soft mooring system has been verified to be applicable.

(3) Gap resonances can be found at wave frequencies between 4s and 8s. The peak periods of both 1-year and 100-year storm locate in this range which will probably lead to green water on the barges. This should be improved in the future. The numerical model correctly predicts the gap resonance peak periods, while the peak values are overestimated.

In the future, the numerical model will be improved by dampening the free surface elevation in the gaps. Analysis of the results from the random wave tests will be carried out to further understand the hydrodynamic behavior of the FHSF system in the realistic sea state.

ACKNOWLEDGMENTS

This research is supported in part by the Singapore Ministry of National Development and the National Research Foundation, Prime Minister's Office under the Land and Liveability National Innovation Challenge (L2 NIC) Research Programme (L2 NIC Award No L2 NICTDF1-2015-2). Any opinions, findings, and conclusions or recommendations expressed in this material are those of the author(s) and do not reflect the views of the Singapore Ministry of National Development and National Research Foundation, Prime Minister's Office, Singapore. The authors acknowledge WAMIT for providing educational license.

REFERENCES

[1] Wang, C., & Wang, B. (2015). Large Floating Structures (pp. 1-36). Springer, Singapore.

[2] Miyajima, S., Seto, H., & Ohta, M. (2003). Hydroelastic responses of the Mega-Float Phase-II model in waves. International Journal of Offshore and Polar Engineering, 13(04).

[3] Cheng, Z., Gao, Z., & Moan, T. (2018). Hydrodynamic load modeling and analysis of a floating bridge in homogeneous wave conditions. Marine Structures, 59, 122-141.

[4] Lamas-Pardo, M., Iglesias, G., & Carral, L. (2015). A review of Very Large Floating Structures (VLFS) for coastal and offshore uses. Ocean Engineering, 109, 677-690.

[5] Wang, C. M., & Tay, Z. Y. (2011). Hydroelastic analysis and response of pontoon-type very large floating structures. In Fluid-structure interaction II (pp. 103-130). Springer, Berlin, Heidelberg.

[6] Watanabe, E., Utsunomiya, T., & Wang, C. M. (2004). Hydroelastic analysis of pontoon-type VLFS: a literature survey. Engineering Structures, 26(2), 245-256.

[7] Newman, J. N. (1994). Wave effects on deformable bodies. Applied ocean research, 16(1), 47-59.

[8] Newman, J. N. (2001). Wave effects on multiple bodies. Hydrodynamics in ship and ocean engineering, 3, 3-26.

[9] Riggs, H. R., Ertekin, R. C., & Mills, T. R. J. (2000). A comparative study of RMFC and FEA models for the wave-induced response of a MOB. Marine structures, 13(4-5), 217-232.

[10] Fu, S., Moan, T., Chen, X., & Cui, W. (2007). Hydroelastic analysis of flexible floating interconnected structures. Ocean Engineering, 34(11-12), 1516-1531.

[11] Liu, Y. H., Kim, C. H., & Lu, X. S. (1990, August). Comparison of higher-order boundary element and constant panel methods for hydrodynamic loadings. In the First ISOPE European Offshore Mechanics Symposium. International Society of Offshore and Polar Engineers.

[12] Zhang, H., Xu, D., Lu, C., Qi, E., Hu, J., & Wu, Y. (2015). Amplitude death of a multi-module floating airport. Nonlinear Dynamics, 79(4), 2385-2394.

[13] Wan, L., Zhang, C., Magee, A. R., Jin, J., Han, M., Ang, K. K., & Hellan, Ø. (2018). An innovative mooring system for

floating storage tanks and stochastic dynamic response analysis. Ocean Engineering, 170, 361-373.
[14] Zhang, C., Magee, A. R., Ling, W., Wang, C. M., & Hellan, Ø. (2017, June). Experimental Study of Hydrodynamic Responses of a Single Floating Storage Tank with Internal Fluid. In ASME 2017 36th International Conference on Ocean, Offshore and Arctic Engineering (pp. V07AT06A058-V07AT06A058). American Society of Mechanical Engineers.
[15] Fonseca, N., Zhang, C., Rodrigues, M., Ren, N., Hellan, Ø., Magee, A. (2019, June). Hydrodynamic model tests with a large floating hydrocarbon storage facility. Submitted to the 38th Int. Con. on Ocean, Offshore & Arctic Eng. OMAE2019, paper 96761, June 9-14, Glasgow, Scotland.
[16] Molin, B. (2001). On the piston and sloshing modes in moonpools. Journal of Fluid Mechanics, 430, 27-50.
[17] Faltinsen, O. Sea Loads on Ships and Offshore Structures. Cambridge University Press, Cambridge, UK, 1990.
[18] Lee, C. H., & Newman, J. N. (2013). WAMIT user manual, version 7.0. WAMIT, Inc., Chestnut Hill, MA.